# Wannier Exciton in an Electric Field. II. Electroabsorption in Direct-Band-Gap Solids

Daniel F. Blossey
*Xerox Research Laboratories, Xerox Square, Rochester, New York,* 14603
(Received 11 August 1970)

The electric field and temperature dependence of excitonic electroabsorption is presented for direct-band-gap semiconductors and insulators. Each excitonic electroabsorption spectrum is characterized in terms of three energy parameters: (i) $R$, the binding energy of the exciton; (ii) $\Gamma$, the thermal broadening parameter; and (iii) $\hbar\theta$, the electro-optical energy. The relative magnitude of these three quantities determines which, if any, of the competing forces dominate. In comparison with the single-particle electroabsorption theory, the excitonic electroabsorption theory gives several new results. The electric field and temperature dependence of $\epsilon_2$, $\Delta\epsilon_2$, and $\Delta\epsilon_1$ are displayed. Fitting of the excitonic electroabsorption theory to lead iodide data gives the values of 2.58 eV for the direct gap in lead iodide and 0.21 electron masses for the reduced mass of the electron-hole pair associated with the extrema in the valence and conduction bands, as compared with previous values of 2.55 eV and 0.24 electron masses.

## I. INTRODUCTION

Several calculations of electric field effects on optical absorption by Wannier excitons have been published in recent years.[1-9] All of these calculations have sought a solution to the quantum-mechanical problem of the hydrogenic atom in an electric field. The fact that there is no known analytic solution to this problem has led the theorists to try approximate models[2,9] and numerical integration[1,3-6] of the differential equation. A Green's-function solution[7] which was presented as an exact solution later proved to be adequate only in the limit of very high fields.[8,9] The results of the models,[2,9] unfortunately, do not bear a close enough resemblance to the real system and only the numerical integrations[1,3-6] have given reasonable results for all values of electric field. A comprehensive study of electric field effects on optical absorption by Wannier excitons was presented in a previous paper,[1] hereafter denoted I, in which field effects on both bound and continuum states were shown. The effect of the electron-hole interaction on the electric-field-induced oscillations in the optical density of states was also demonstrated with the result that the electron-hole interaction enhances these oscillations near an $M_0$-type edge (positive effective masses) and quenches these oscillations near an $M_3$-type edge (negative effective masses). It was suggested that this effect would inhibit the observation of $M_3$-type edges in electroreflectance. The most glaring deficiency of all these calculations[1-9] is that not one of them has been put in a form such that it can be compared with a modulated spectrum, i.e., an electroabsorption or an electroreflectance spectrum.[10] It is to this deficiency that we address ourselves in this paper.

Modulated spectroscopy, particularly electroabsorption (EA) and electroreflectance (ER), has generated a great deal of information about the electronic band structure of solids. This technique, under the name of electric-field-induced spectroscopy (EFS), has also been applied to the electronic spectra of gaseous molecules and has generated extremely well-resolved rotational structure.[11] In this paper, we will concentrate on the EA spectrum near the fundamental edge of direct-band-gap solids. Figure 1 shows a simple two-band model for a direct-band-gap solid and the resulting absorption spectrum near the direct edge. The exact position of the edge, as shown in Fig. 1, is somewhat hard to pinpoint. The EA spectrum gives much better resolution as well as additional information about band anisotropy and effective masses. Figure 2 shows the electric-field-induced oscillations in the optical density of states and the EA spectrum with its strongest structure about the energy gap $E_g$. This spectrum is measured using standard phase-sensitive techniques.[10] The temperature and field dependence of the excitonic EA spectrum will be demonstrated later in the paper but first it is useful

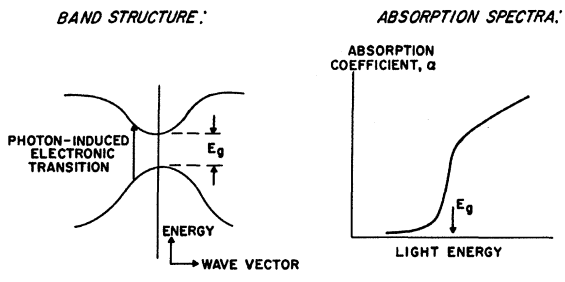


FIG. 1. Simple two-band model for direct-band-gap solid and resulting absorption spectrum near the fundamental edge.

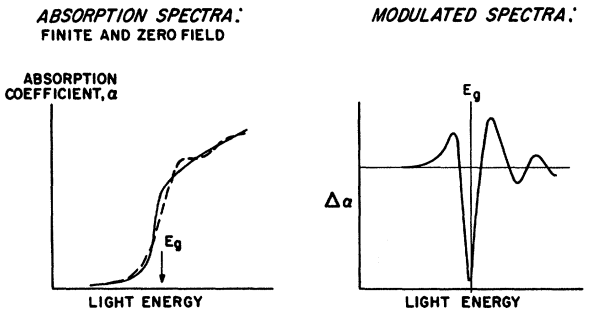


FIG. 2. Electric-field-induced oscillations in the optical density of states near the fundamental edge and the resulting electroabsorption spectrum representing the difference between the finite- and zero-field absorption curves.

to review some basic concepts of Wannier exciton theory and electric field effects.

The Wannier exciton is an electron-hole pair created by photoexcitation of a crystalline solid.[12–15] This type of exciton is a hydrogenic atom typified by the effective masses of the electron and hole and by the dielectric constant of the solid. This model for the exciton is applicable to crystals which can generate charge carriers upon exposure to light, i.e., photoconductors. Also, from the formalism of the theory, it is required that the effective size of the excitation cover several unit cells of the crystal. The size of the excitation is related to how much an electron is shared among the various lattice sites. For covalently bonded crystals, the electron is shared equally among many sites and, consequently, the excitation covers many sites; but, for ionic, molecular, and rare-gas solids, the electronic motion is much more restricted and the excitations are thereby more localized. These localized excitations are generally called Frenkel excitons.[16–20] Thus, the Wannier theory for excitons is primarily applicable to semiconducting crystals,[21] particularly from group IV of the Periodic Table; many of the more qualitative results of this theory are applicable to noncovalently bonded crystals.[20]

The Wannier exciton in the effective-mass approximation is equivalent to the hydrogen atom differing only in the values of the effective masses of the electron and hole and the dielectric constant of the medium.[13] The bound states of the electron-hole pair occur in the forbidden gap of semiconductors and insulators at energies given by

$$E_n = E_g - Rn^{-2}, \tag{1}$$

where $E_g$ is the energy gap and $R$ is the effective Rydberg energy. The intensities of the absorption lines for these bound levels are proportional to $n^{-3}$. These lines blend into a quasicontinuum for energies very near but just below the gap energy and then become a true continuum above the gap. The effective Rydberg $R$ is given by

$$R = \frac{\mu e^4}{2\hbar^2\epsilon^2} = \left(\frac{\mu}{m}\right) \times \epsilon^{-2} \times 13.6 \text{ eV}, \tag{2}$$

where $\mu$ is the reduced mass of the electron-hole pair, $m$ is the electronic mass, and $\epsilon$ is the static dielectric constant of the solid. The radius (effective Bohr radius) of the exciton is given by

$$a = \frac{\hbar^2\epsilon}{\mu e^2} = \left(\frac{\mu}{m}\right)^{-1} \times \epsilon \times 5.29 \times 10^{-9} \text{ cm}. \tag{3}$$

Thus, we see that a small effective mass (highly mobile carriers) and a large dielectric constant both combine to give large radii for the excitons which is one of the criteria for validity of the Wannier theory.

Since the Coulomb potential is altered by the dielectric constant $\epsilon$, the electron-hole pair in an electric field sees the combined potential

$$V(r) = -e^2/\epsilon r - e\vec{\mathcal{E}} \cdot \vec{r}\,, \tag{4}$$

where $\vec{r} = \vec{r}_e - \vec{r}_h$ and $\vec{\mathcal{E}}$ is the electric field. This potential is shown in Fig. 3 for zero and finite electric fields. The major effect of the electric field is to lower the lip of the potential well which causes the bound levels to be mixed and broadened into a continuum. A secondary effect of the electric field is a slight widening of the Coulomb well which causes a shift of the 1$s$ level to lower energies which produces the well-known phenomena of the second-order Stark shift. For the electric field to be capable of ionizing the exciton, it must provide at least a potential drop of 1 Ry across the effective Bohr radius; this ionization field $\mathcal{E}_I$ is defined as

$$\mathcal{E}_I = R/ea = (\mu^2/m) \times \epsilon^{-3} \times 2.59 \times 10^9 \text{ V/cm}. \tag{5}$$

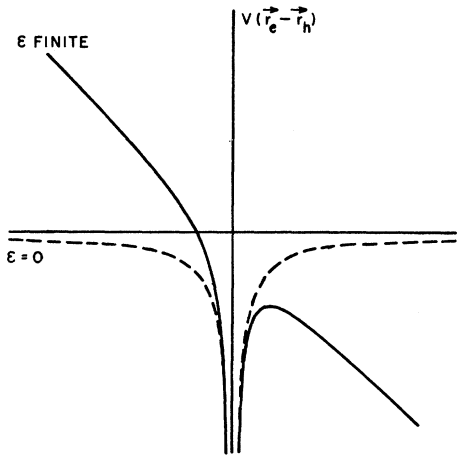


FIG. 3. Electron-hole interactions with and without externally applied electric field.

TABLE I. Energy gaps, exciton binding energies (exciton associated highest-energy split-off valence band), and ionization fields for various semiconductors and insulators.

| Crystal | $E_g$(eV) | $R$(meV) | $\mathcal{E}_I(10^3$ V/cm) |
|---|---|---|---|
| InSb | 0.2357 | 0.5 | 0.08 |
| InAs | 0.360 | 1.8 | 0.70 |
| Ge | 0.800 | 1.4 | 0.55 |
| GaSb | 0.813 | 1.8 | 1.00 |
| InP | 1.29 | 6.5 | 7.8 |
| GaAs | 1.41 | 5.1 | 5.7 |
| AlSb | 1.6 | 7.5 | 12 |
| CdTe | 1.606 | 10.0 | 31 |
| CdSe | 1.8415 | 15.7 | 60 |
| ZnTe | 2.301 | 13.0 | 47 |
| $PbI_2$ | 2.55 | 73.0 | 460 |
| CdS | 2.5831 | 29.4 | 140 |
| ZnSe | 2.818 | 19.0 | 75 |
| ZnS | 3.9115 | 40.1 | 200 |

In Table I, there is a listing of energy gaps, binding energies, and ionization fields for various semiconductors and insulators calculated from tabulated values of effective masses and dielectric constants[22–26]; the crystals are ordered by increasing value of energy gap.

There are very few published calculations of electric field effects on the hydrogenic atom. For calculation of Stark shifts and splittings,[27–30] perturbation methods are appropriate if $\mathcal{E}/\mathcal{E}_I \ll 1$. But for electric fields on the order of or larger than $\mathcal{E}_I$, the electric field dominates the Coulomb potential and a nonperturbative solution is needed. The first nonperturbative approach was proposed by Duke and Alferieff[2] in which they reduced the electric field plus Coulomb potentials to the analytically solvable model of only the Coulomb potential inside a given radius and only the electric field potential outside the given radius. This model is adequate in the high-field limit but fails to predict correct Stark shifts in the low-field limit. To improve on the results of Duke's model, numerical integrations of the hydrogenic Schrödinger equation have been performed by Ralph,[3] Dow and Redfield,[4] and the author.[1,5,6] Ralph[3] calculated the shifts and broadenings of the 1$s$ hydrogenic level and Dow and Redfield[4] demonstrated the electric field dependence of the excitonic absorption tail in the band gap and compared this with Urbach's rule. Enderlein[7] used a Green's-function approach to solve the problem but one of his assumptions made his results valid only in the limit of $\mathcal{E} \gg \mathcal{E}_I$.[8,9]

The field dependence of $\epsilon_2$ for excitonic absorption has been calculated in paper I.[1] In Secs. II and III, we will be examining the field and temperature dependence of the excitonic EA spectrum.[10] This involves calculating a properly normalized zero-field spectrum as well as a finite-field spectrum and taking the difference. The dielectric functions $\epsilon_2(\mathcal{E})$ and $\epsilon_2(0)$ will be displayed as functions of temperature and electric field in Sec. II A. The field-induced changes $\Delta\epsilon_2$ and $\Delta\epsilon_1$ will be displayed as functions of temperature and electric field in Secs. II B and II C, respectively. Fits to lead iodide EA data will be shown in Sec. II D and the thermally ionized exciton limit is considered in the Appendix. A discussion of the results is contained in Sec. III.

## II. ELECTROABSORPTION

Since the early work (1958) of Franz[31] and Keldysh[32] on photon-assisted tunneling between bands, the theory of EA has progressed a long way. These early theories[31,32] presented an asymptotic formula for electric-field-induced optical absorption in the forbidden gap and predicted a red shift of the band edge with field. The first published experimental work appeared two years later and showed a field-induced shift to lower energies of an exponential absorption edge in CdS.[33] Similar results appeared two years later (1962) for GaAs.[34] The following year, Tharmalingam[35] presented a closed form solution which agreed with the Franz-Keldysh theory below the edge and showed electric-field-induced oscillations in the optical density of states above the edge. Similar results were obtained by Callaway[36] using field-dependent electron and hole wave functions.[37] The equivalence of these two theories was not demonstrated until several years later (1968) by Aspnes, Handler, and Blossey[38] in which a more general expression for EA was derived. The electric-field-induced oscillations were first observed in EA by Frova and Handler[39] and in ER by Seraphin.[40] Since then a deluge of experimental data has appeared in the literature.[10] Experimentalists have attempted to fit EA data to the nonexcitonic EA theory[38,41] with some success. Qualitative but not quantitative agreement could be achieved. In 1966, Hamakawa, Germano, and Handler[42] suggested that exciton effects were the dominate cause of discrepancies between EA theory and experiment. They later showed that only one of the six possible predictions of the nonexcitonic EA theory was confirmed by experiment.[43] Additional work on CdS[44] and $PbI_2$,[45,46] in which exciton absorption is known to dominate the spectra, confirmed that the nonexcitonic EA theory was inadequate. Sec. II A will contain the first display of theoretical excitonic EA spectra as functions of electric field and temperature and a fit to the lead iodide EA data of Perov *et al.*[46]

### A. Zero- and Finite-Field Absorption

It was shown in I that the imaginary part of the dielectric constant $\epsilon_2$ may be expressed as

$$\epsilon_2 = \tfrac{4}{3}\epsilon \left| \vec{\mu}_{cv}/ea \right|^2 \phi^2(0) \tag{6}$$

for absorption near the direct edge where $\epsilon$ is the static dielectric constant, $\vec{\mu}_{cv}$ is an interband dipole-matrix element, $a$ is the exciton radius, and $\phi^2(0)$ is the density-of-states function. The interband dipole-matrix element $\vec{\mu}_{cv}$ is defined in terms of an interband momentum-matrix element $\vec{P}_{cv}$, where

$$\vec{\mu}_{cv} = (e/m\omega)\vec{P}_{cv} = (e/m\omega)\langle \psi_c | \langle \hbar/i \rangle \nabla | \psi_v \rangle . \tag{7}$$

The $\psi_c$ and $\psi_v$ are the Bloch states for the conduction and valence bands, respectively. From Eq. (6), it is evident that the square of the ratio of the transition dipole moment to the exciton dipole moment determines the strength of the exciton absorption. The density-of-states function $\phi^2(0)$, which contains all electric-field-induced structure, is dimensionless and is normalized to approach the limit $[(\hbar\omega - E_g)/R]^{1/2}$ far above the edge. For electric field $\mathcal{E} = 0$, the density-of-states function includes the hydrogenic series below the edge and blends into a continuum above the edge. Thus, from I, in the zero-field limit, $\phi^2(0)$ is given by

$$\phi^2(0) = 4\pi \sum_{n=1}^{\infty} n^{-3}\, \delta\left(\frac{\hbar\omega - E_g + Rn^{-2}}{R}\right), \quad \hbar\omega < E_g \tag{8a}$$

$$\phi^2(0) = \frac{2\pi}{1 - e^{-2\pi[(\hbar\omega - E_g)/R]^{-1/2}}}, \quad \hbar\omega > E_g . \tag{8b}$$

Below the edge, $\phi^2(0)$ contains the hydrogenic series with each line having strength $4\pi n^{-3}$. Near the edge, both expressions approach the limit $\phi^2(0) = 2\pi$, below the edge as a quasicontinuum and above the edge as a continuum. Far above the edge, $\phi^2(0)$ approaches the desired limit of $[(\hbar\omega - E_g)/R]^{1/2}$. For $\mathcal{E} \neq 0$, $\phi^2(0)$ is expressed in terms of parabolic coordinate eigenfunctions $f_{\kappa_i}$ and $g_{\kappa_i'}$ as

$$\phi^2(0) = \left(\frac{\mathcal{E}}{\mathcal{E}_I}\right)^{1/3} \sum_{i=1}^{\infty} f_{\kappa_i}^2(0)\, g_{\kappa_i'}^2(0), \tag{9}$$

where $f_\kappa$ and $g_{\kappa'}$ are solutions of the differential equations

$$\frac{1}{x}\frac{d}{dx}\left(x\frac{d}{dx}\begin{bmatrix} f \\ g \end{bmatrix}\right) + \left(-\frac{1}{x}\begin{bmatrix} \kappa \\ \kappa' \end{bmatrix} + \beta - x\right)\begin{bmatrix} f \\ g \end{bmatrix} = 0, \quad \begin{bmatrix} x > 0 \\ x < 0 \end{bmatrix} \tag{10}$$

where $\kappa' = \kappa + 2(\mathcal{E}/\mathcal{E}_I)^{-1/3}$,

$$\beta = (\mathcal{E}/\mathcal{E}_I)^{-2/3}[(E - E_g)/R],$$

and the $\kappa_i$ are the allowed eigenvalues as continuous functions of $\beta$. The solutions of Eq. (10) and the various parameter definitions are fully documented in I and need not be belabored here. All that need be said is that Eq. (10) is numerically integrable and that computer programs have been written to do this. The consistency of normalization between the zero- and finite-field curves will become clear below.

To be able to compare theory with experiment, a phenomenological broadening factor $\Gamma \sim kT$ must be introduced. The author tried both Gaussian- and Lorentzian-type broadenings and found that the Lorentzian-type correlated best with experimental data.[47] The Lorentzian broadening of Eqs. (8a) and (8b) can be accomplished analytically, whereas the broadening of Eq. (9) must be accomplished numerically. Upon broadening Eqs. (8a) and (8b), the two equations may be combined into one for the broadened zero-field curve. The temperature and field dependence of $\phi^2(0)$ or $\epsilon_2$ is shown in Fig. 4. Each figure is for a given value of $\Gamma/R$ and contains three curves, one for zero field and two for nonzero values of $\mathcal{E}/\mathcal{E}_I$; the numbers on the curves correspond to different values of this parameter. The relationship between the electro-optical energy $\hbar\theta$, the exciton binding energy $R$, the electric field $\mathcal{E}$, and the ionization field $\mathcal{E}_I$ is simply

$$\hbar\theta/R = (\mathcal{E}/\mathcal{E}_I)^{2/3}. \tag{11}$$

The consistency of normalization between the zero- and finite-field curves is fully demonstrated by Fig. 4, in that the oscillations above the edge are centered on the zero-field curve as they should be. This is somewhat remarkable considering that the finite-field curves were calculated numerically from Eqs. (9) and (10), whereas the zero-field curves were calculated analytically from Eqs. (8a)

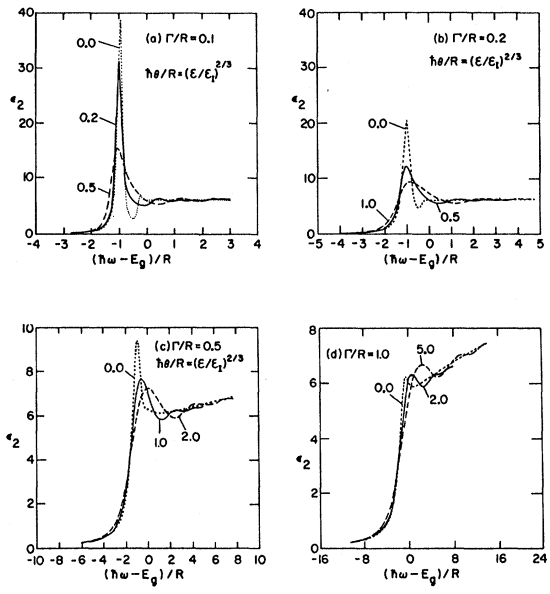


FIG. 4. Temperature and electric field dependence of $\epsilon_2$ as function of $(E - E_g)/R$ for (a) $\Gamma/R = 0.1$, $\mathcal{E}/\mathcal{E}_I = 0.0$, 0.2, and 0.5; (b) $\Gamma/R = 0.2$, $\mathcal{E}/\mathcal{E}_I = 0.0$, 0.5, and 1.0; (c) $\Gamma/R = 0.5$, $\mathcal{E}/\mathcal{E}_I = 0.0$, 1.0, and 2.0; and (d) $\Gamma/R = 1.0$, $\mathcal{E}/\mathcal{E}_I = 0.0$, 2.0, and 5.0.

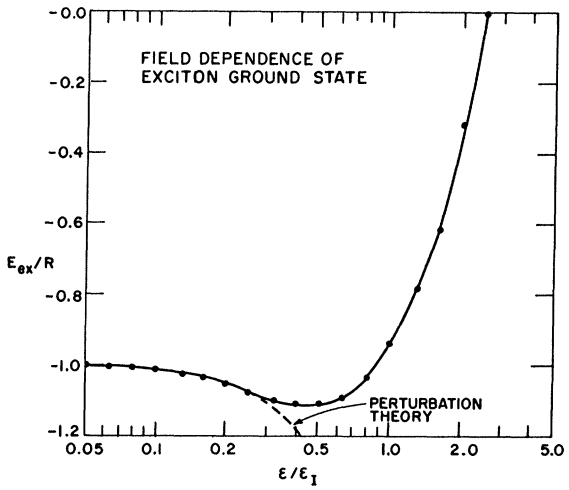


FIG. 5. Field dependence of exciton (hydrogenic) ground-state energy.

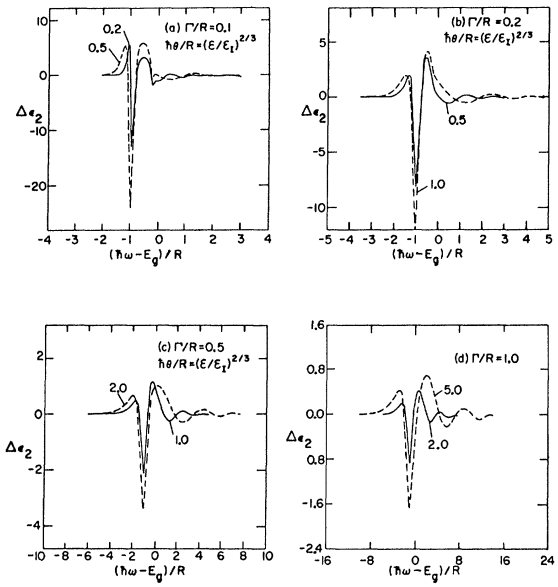


FIG. 6. Temperature and electric field dependence of $\Delta\epsilon_2$ as function of $(E-E_g)/R$ for (a) $\Gamma/R=0.1$, $\mathcal{E}/\mathcal{E}_I=0.2$ and 0.5; (b) $\Gamma/R=0.2$, $\mathcal{E}/\mathcal{E}_I=0.5$ and 1.0; (c) $\Gamma/R=0.5$, $\mathcal{E}/\mathcal{E}_I=1.0$ and 2.0; and (d) $\Gamma/R=1.0$, $\mathcal{E}/\mathcal{E}_I=2.0$ and 5.0.

and (8b) with no adjustable scaling factors. The consistency of normalization is also demonstrated by conservation of total oscillator strengths ($f$ sum rule). This consistency is especially important because, to calculate the modulated spectrum, one must take the difference between the finite- and zero-field spectra.

The field dependence of the exciton (hydrogenic) ground-state energy is shown in Fig. 5. The peak follows the quadratic Stark shift up to a field of about $0.25\,\mathcal{E}_I$. A minimum energy is obtained in the $0.4\mathcal{E}_I$–$0.5\mathcal{E}_I$ range and the peak moves to higher energies above $0.5\mathcal{E}_I$. For $\mathcal{E}/\mathcal{E}_I>1$, the peak exists only as the first electric-field-induced oscillation in the optical density of states. The broadening due to the electric field is demonstrated in Fig. 7 of I.

### B. Field-Induced Changes in $\epsilon_2$

Several theoretical excitonic EA spectra, represented by $\Delta\epsilon_2$, are shown in Fig. 6. These curves were evaluated by taking the difference between the finite- and zero-field spectra of Fig. 4. As the field increases, the excitonic EA spectrum expands as $(\mathcal{E}/\mathcal{E}_I)^{2/3}$ above the edge with the first negative oscillation being pinned at $\hbar\omega=E_g-R$ if the exciton is not thermally ionized ($\Gamma<R$). The temperature and field dependence of amplitudes and energy separations in $\Delta\epsilon_2$ are shown in Figs. 7 and 8. From the field and temperature dependence of these EA parameters, several predictions can be made: (a) $h_3$ should be greater than $h_1$ except for the case of both small field ($\mathcal{E}/\mathcal{E}_I<0.3$) and small broadenings ($\Gamma/R<0.2$); (b) $h_1$ and $h_3$ can increase or decrease with field whereas $h_2$ should always increase with field; (c) for large fields, $h_2$ should approach a constant value if the exciton is not thermally ionized; (d) when the exciton is neither field or thermally ionized, the first negative oscillation is pinned at $\hbar\omega=E_g-R$; (e) the width $\Delta E_1$ increases slower than $(\mathcal{E}/\mathcal{E}_I)^{2/3}$ and is temperature dependent, whereas the width $\Delta E_2$ increases as $(\mathcal{E}/\mathcal{E}_I)^{2/3}$ and is largely temperature independent. It should be emphasized that these results are for nondegenerate bands. For overlapping bands, the effects are generally additive.[48] The above predictions have been borne out qualitatively by experiment.[43] A quantitative comparison between lead iodide EA data and the

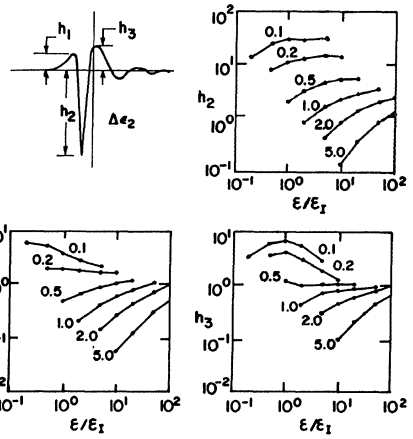


FIG. 7. Temperature and electric field dependence of amplitudes in $\Delta\epsilon_2$ for $\Gamma/R=0.1$, 0.2, 0.5, 1.0, 2.0, and 5.0.

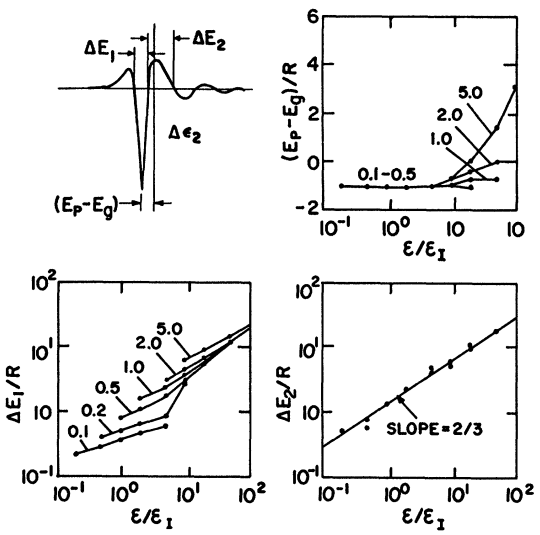


FIG. 8. Temperature and electric field dependence of energy differences in $\Delta\epsilon_2$ for $\Gamma/R=0.1$, 0.2, 0.5, 1.0, 2.0, and 5.0.

excitonic EA theory is made in Sec. IID.

### C. Field-Induced Changes in $\epsilon_1$

Using the Kramers-Kronig relationships, $\Delta\epsilon_1$ may be calculated from $\Delta\epsilon_2$; $\Delta\epsilon_1$ is important since both $\Delta\epsilon_1$ and $\Delta\epsilon_2$ contribute to the ER spectrum. Several $\Delta\epsilon_1$ curves are shown in Fig. 9. These curves are calculated, assuming $R \ll E_g$, from the $\Delta\epsilon_2$ curves in Fig. 6. The $\Delta\epsilon_1$ spectrum expands approximately as $(\mathcal{E}/\mathcal{E}_I)^{2/3}$, as does the $\Delta\epsilon_2$ spectrum, with the first zero below the edge being pinned at

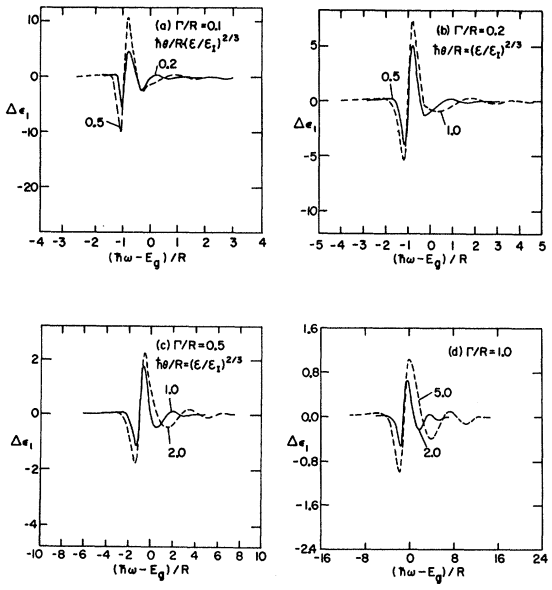


FIG. 9. Temperature and electric field dependence of $\Delta\epsilon_1$ as function of $(E-E_g)/R$ for (a) $\Gamma/R=0.1$, $\mathcal{E}/\mathcal{E}_I=0.2$ and 0.5; (b) $\Gamma/R=0.2$, $\mathcal{E}/\mathcal{E}_I=0.5$ and 1.0; (c) $\Gamma/R=0.5$, $\mathcal{E}/\mathcal{E}_I=1.0$ and 2.0; and (d) $\Gamma/R=1.0$, $\mathcal{E}/\mathcal{E}_I=2.0$ and 5.0.

$\hbar\omega = E_g - R$ if the exciton is not thermally ionized. The field and temperature dependence of amplitudes and energy separations in $\Delta\epsilon_1$ are shown in Figs. 10 and 11. From the field and temperature dependence of these $\Delta\epsilon_1$ parameters, several predictions can be made: (a) $h_2$ and $h_3$ should be about the same size with $h_2 > h_3$ for high fields; (b) $h_1$ is small relative to $h_2$ and $h_3$; (c) $h_3$ can increase or decrease depending on field, whereas $h_2$ always should increase with field; (d) $h_2$ saturates for $\mathcal{E} > \mathcal{E}_I$ and small broadenings; (e) for small fields ($\mathcal{E}/\mathcal{E}_I < 1$) or small broadenings ($\Gamma/R < 0.5$) the first zero is pinned at $\hbar\omega = E_g - R$ irrespective of field; (f) the widths $\Delta E_1$ and $\Delta E_2$ increase slightly slower than $(\mathcal{E}/\mathcal{E}_I)^{2/3}$ with $\Delta E_2$ approaching this limit at high fields; (g) the width $\Delta E_1$ is less temperature dependent than $\Delta E_2$ at low fields but is more temperature dependent at high fields. In many cases the ER spectra are largely composed of $\Delta\epsilon_1$; thus, in these cases, these results can be directly correlated with ER data.

### D. Comparison with Experiment: Lead Iodide

For comparison between theory and experiment, the lead iodide EA data of Perov *et al.*[46] was used. This data was chosen in preference to CdS[44] or Ge data[43] because of the lack of overlapping structure, which in the case of CdS complicates the EA spectrum. Also, $PbI_2$ exhibits a stronger exciton peak than Ge which should provide a good test for an excitonic EA theory. The fit of both the excitonic and nonexcitonic EA theories to experiment is shown in Figs. 12 and 13. The theoretical curves in these figures were generated using the parameters $\Gamma = kT$, $T = 77\,^\circ$K, $\epsilon = 6.25$, $\mu = 0.21 m_e$, and the electric fields $\mathcal{E} = 8\times10^4$ V/cm and $2.85\times10^5$ V/cm, respectively. The energy-gap values used were 2.58 and 2.48 eV for the excitonic and nonexcitonic theories, respectively.

At best, the nonexcitonic theory gives a poor fit.

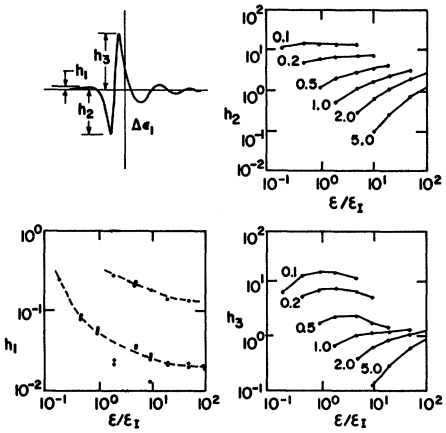


FIG. 10. Temperature and electric field dependence of amplitudes in $\Delta\epsilon_1$ for $\Gamma/R=0.1$, 0.2, 0.5, 1.0, 2.0, and 5.0.

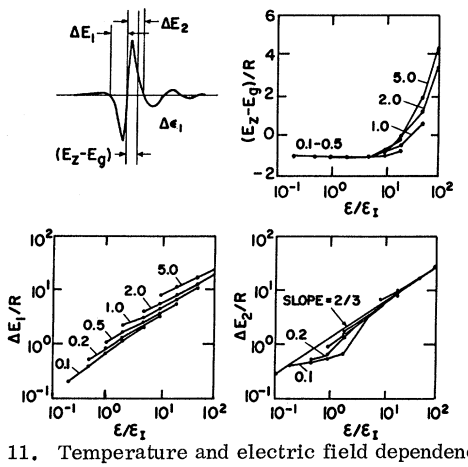


FIG. 11. Temperature and electric field dependence of energy differences in $\Delta\epsilon_1$ for $\Gamma/R = 0.1$, 0.2, 0.5, 1.0, 2.0, and 5.0.

There are many points of discrepancy between the non-excitonic theory and experiment: (a) the calculated energy gap is lower in energy than the first exciton absorption peak (a ridiculous result); (b) the oscillations are too narrow for the smaller field and too wide for the larger field: (c) the oscillation amplitudes are not damped sufficiently above the edge; (d) the first negative half-oscillation is too narrow and deep to fit with the nonexcitonic EA theory. As is clearly demonstrated by Figs. 12 and 13, the excitonic EA theory gives a much better fit to $PbI_2$ EA data than the nonexcitonic EA theory. The nonexcitonic EA theory is treated in the Appendix as the thermally ionized limit of the excitonic EA theory.

Considering the simplicity of the exciton model, the fit of the excitonic EA theory to experiment is quite good. Using these parameters, the ionization field as defined by Eq. (5) is calculated to be $4.67\times10^5$ V/cm in which case $\mathcal{E}/\mathcal{E}_I = 0.17$ and 0.61 for the two figures. For comparison between theory and experiment, 42 curves for different values of electric field ranging from $\mathcal{E}/\mathcal{E}_I = 0.079$ to 1000.0 have been calculated and placed in direct access storage on the computer. The theoretical curves in Figs. 11 and 12 correspond to values of $\mathcal{E}/\mathcal{E}_I = 0.16$ and 0.63, respectively, since these values of $\mathcal{E}/\mathcal{E}_I$ were the closest of the 42 stored curves to the actual values of $\mathcal{E}/\mathcal{E}_I$. The general features of the EA data are reproduced by the theory. For example, in the case of the lower field ($8\times10^4$ V/cm), $h_1$ is almost two times $h_3$; whereas, in the case of the higher field ($2.85\times10^5$ V/cm), $h_1$ is less than $h_3$. In both cases, the magnitudes of $h_1$, $h_2$, and $h_3$ are in the right proportions to fit the theory to the experimental data. The oscillations above the edge are not quite in phase which may be due to the oversimplification of the electron-hole interaction as being simply a Coulomb potential. In actuality, the electron and hole are not point particles and can overlap if they are in the same unit cell. This effect causes the potential well to have a bottom, and thereby causes deviations from the hydrogenic series. The greatest weight of the fit was placed on the first three half-oscillations which would cause a difference of phase in the oscillations above the edge if the exciton series is not purely hydrogenic. From Fig. 13, the exciton peak in $PbI_2$ seems to be about 0.02 eV higher than that which would be predicted by the hydrogenic model.

## III. DISCUSSION

If the excitonic and nonexcitonic (single-particle) EA theories are to be compared, there are several points that need clarification. Since the EA spectrum is the difference between a finite-field spectrum and a zero-field spectrum, the EA spectrum contains structure from both spectra. In the case of the nonexcitonic EA theory, the zero-field spectrum contributes little structure except at the fundamental edge where a singularity in $\epsilon_2$ occurs. In contrast, the zero-field exciton spectrum can contain many absorption peaks corresponding to the bound exciton states. This structure is absent only if the thermal broadening is much greater than the exciton binding energy, in which case the nonexcitonic EA theory is applicable (see the Appendix). The electric field induces spectral shifts and broadenings of any structure in the zero-field spectrum and causes electric-field-induced oscillations in the optical density of states above the edge. The electron-hole interaction enhances these oscillations near the edge and causes a phase shift in energy there. The nonexcitonic EA spectrum expands as $\mathcal{E}^{2/3}$, whereas only the part of the excitonic EA spectrum above the edge follows this power law. Below the edge, the excitonic EA spectrum is dominated by the structure in the zero-field spectrum. The excitonic EA theory introduces an additional

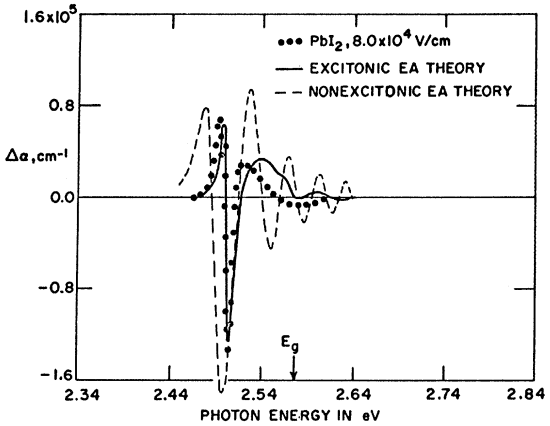


FIG. 12. Fit of excitonic and nonexcitonic electroabsorption theories to lead iodide data of Perov *et al.* (Ref. 46) for electric field of $8\times10^4$ V/cm at 77 °K.

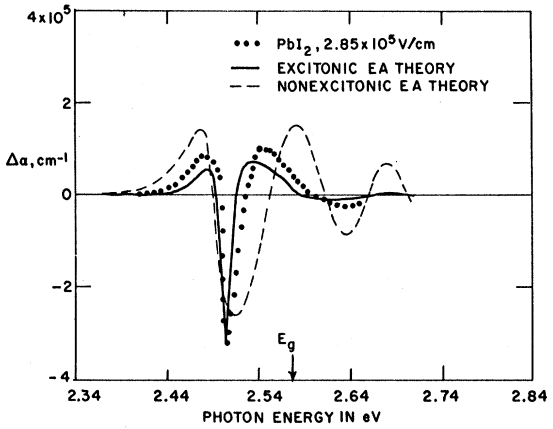


FIG. 13. Fit of excitonic and nonexcitonic electroabsorption theories to lead iodide data of Perov *et al.* (Ref. 46) for electric field at $2.85\times10^5$ V/cm at 77 °K. Both theoretical curves in this and the previous figure used the parameters $\Gamma = kT$, $E_g = 2.58$ eV, and an electron-hole-pair reduced mass $\mu = 0.21 m_e$.

complication in characterization of the EA spectrum, i.e., the single-particle EA theory can be characterized by the energy parameters $\Gamma$, the thermal broadening energy $\hbar\theta$, the electro-optical energy, and $E_g$, the energy gap, whereas the excitonic EA theory also includes $R$, the binding energy of the exciton.

In this theory, the electron-hole interaction is treated as a Coulomb potential between point particles. It has already been pointed out in the text that this potential tends slightly to overestimate the exciton binding energy owing to the fact that the particles are actually charge densitites covering entire unit cells of the crystal and not point particles. But to make the problem tractable certain simplifying approximations must be introduced, such as the Coulomb potential for the electron-hole interaction and effective masses for the band structure. Even with these approximations the agreement between theory and experiment is quite good. The reduced mass of the electron-hole pair $\mu$ along with static dielectric constant $\epsilon$ of the solid combine to define the exciton binding energy $R$ and the exciton radius $a$. The exciton radius in lead iodide is about 16 Å, thus making it a marginal case for study by Wannier exciton theory which requires that the exciton span several unit cells of the crystal. Even so, a good fit was obtained. From the best fit to EA data for two different values of electric field, the parameters $E_g = 2.58$ eV, $\mu = 0.21 m_e$ were obtained for $\epsilon = 6.25$ and $\Gamma = kT$, where $T = 77$ °K for lead iodide which are in reasonable agreement with previous values of 2.55 eV and $0.24 m_e$.[45]

In summary, the electric field and temperature dependence of excitonic EA is presented in graphical form for direct band-gap semiconductors and insulators. Each excitonic EA spectrum is characterized in terms of ratios of three parameters $R$, $\Gamma$, and $\hbar\theta$, the magnitude of each relative to one another determining which, if any, of the competitive forces dominate. In only one case does the excitonic EA theory agree with the nonexcitonic theory – the oscillations in the optical density of states above the edge expand as $\mathcal{E}^{2/3}$. This theory explains many of the features of measured EA spectra which are inconsistent with the nonexcitonic EA theory such as temperature-dependent and field-independent oscillations and hitherto anomolous dependencies of the amplitudes of the oscillations on field.[43]

## APPENDIX: ELECTROABSORPTION BY THERMALLY IONIZED ELECTRONS

In the limit of large thermal broadening of the exciton lines $\Gamma \gg R$, the excitonic EA spectrum approaches the nonexcitonic EA spectrum. The broadened nonexcitonic EA spectrum may be expressed in terms of complex Airy functions[41] which are Bessel functions of fractional order.[49] The complex Airy function is the analytic continuation of the convergent real-axis solution of the equation[49]

$$\frac{d^2}{dz^2}\,\mathrm{Ai}(z) = z\,\mathrm{Ai}(z) \tag{12}$$

whose integral representation is given by[50]

$$\mathrm{Ai}(z) = \frac{1}{\pi}\int_0^\infty ds\, e^{-(1/2)sz-(1/3)s^3}\cos(\tfrac{1}{2}\sqrt{3}\,sz+\tfrac{1}{6}\pi). \tag{13}$$

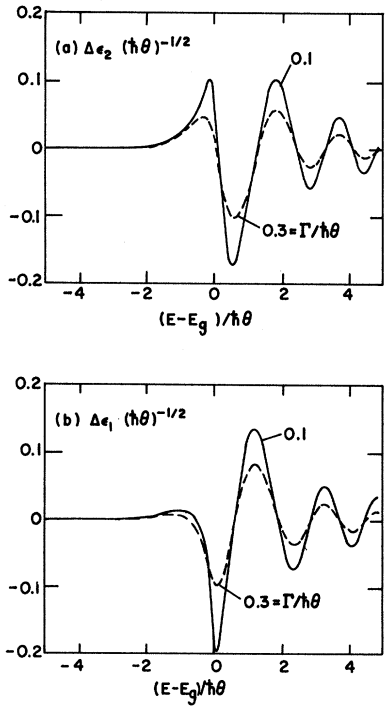


FIG. 14. Electroabsorption spectra for thermally ionized excitons, $\Gamma \gg R$: (a) $\Delta\epsilon_2$ vs $(E-E_g)/\hbar\theta$ for $\Gamma/\hbar\theta = 0.1$ and 0.3; (b) $\Delta\epsilon_1$ vs $(E-E_g)/\hbar\theta$ for $\Gamma/\hbar\theta = 0.1$ and 0.3.

For completeness, a second solution to Eq. (12) is Bi($z$) whose integral representation is given by[50]

$$\mathrm{Bi}(z)=\frac{1}{\pi}\int_0^\infty ds\, e^{-(1/2)sz-(1/3)s^3}\sin(\tfrac{1}{2}\sqrt{3}\,sz+\tfrac{1}{6}\pi)+\frac{1}{\pi}\int_0^\infty ds e^{sz-(1/3)s^3}. \quad (14)$$

The complex functions Ai($z$) and Bi($z$) are interrelated by the formula[49]

$$\mathrm{Ai}(z)+i\mathrm{Bi}(z)=2e^{i\pi/3}\,\mathrm{Ai}(ze^{-i2/3}). \quad (15)$$

For EA calculations, we have that in the limit of $\Gamma \gg R$

$$\phi^2(0)\sim(\mathcal{E}/\mathcal{E}_I)^{1/3}\,2\pi\,\mathrm{Re}[e^{-i\pi/3}\mathrm{Ai}'(z)\mathrm{Ai}'(ze^{-i2\pi/3})+ze^{-i2\pi/3}\mathrm{Ai}(z)\mathrm{Ai}(ze^{-i2\pi/3})] \quad (16)$$

for finite fields and broadenings where $\mathrm{Ai}'(z)=(d/dz)\mathrm{Ai}(z)$ and the zero-field limit is given by

$$\phi^2(0)\sim 2^{-1/2}\left\{\left(\frac{\hbar\omega-E_g}{R}\right)+\left[\left(\frac{\hbar\omega-E_g}{R}\right)^2+\left(\frac{\Gamma}{R}\right)^2\right]^{1/2}\right\}^{1/2},$$

where $\hbar\omega$ is the photon energy, $E_g$ is the energy gap, $R$ is the exciton binding energy, and $\Gamma$ is the thermal broadening energy. The complex parameter $z$ may be expressed in terms of physical parameters as

$$z=(\mathcal{E}/\mathcal{E}_I)^{-2/3}\,[(E_g-\hbar\omega)+i\Gamma]/R=[(E_g-\hbar\omega)+i\Gamma]/\hbar\theta, \quad (18)$$

where $\hbar\theta$ is the electro-optical energy. The modulated spectrum $\Delta\epsilon_2$ representing the difference between Eqs. (16) and (17) is shown in Fig. 14 with its Kramers-Kronig transform $\Delta\epsilon_1$ for two values of $\Gamma/\hbar\theta$. The energy coordinate expands as $\mathcal{E}^{2/3}$ and the first negative oscillation in $\Delta\epsilon_2$ occurs above the gap in contrast to the limit $\Gamma < R$, where the first negative oscillation is pinned at $\hbar\omega = E_g - R$. This theory was used to generate the nonexcitonic curves in Figs. 12 and 13.


[1]D. F. Blossey, Phys. Rev. B 2, 3976 (1970).

[2]C. B. Duke and M. E. Alferieff, Phys. Rev. 145, 583 (1966).

[3]H. I. Ralph, J. Phys. C 1, 378 (1968).

[4]J. D. Dow and D. Redfield, Phys. Rev. B 1, 3358 (1970).

[5]D. F. Blossey, Bull. Am. Phys. Soc. 14, 429 (1969).

[6]D. F. Blossey, Ph.D. thesis, University of Illinois, Urbana, Ill., 1969 (unpublished).

[7]R. Enderlein, Phys. Status Solidi 26, 509 (1968).

[8]J. D. Dow, Phys. Status Solidi 34, K71 (1969).

[9]C. M. Penchina, J. K. Pribram, and J. Sak, Phys. Rev. 188, 1240 (1969).

[10]The term electroabsorption as it is used here refers to the electric-field-modulated spectrum which is the difference between the finite- and zero-field spectra. Reviews on the various aspects of modulated spectroscopy may be found in M. Cardona, in *Solid State Physics*, edited by F. Seitz, D. Turnbull, and H. Ehrenreich (Academic, New York, 1969), Suppl. 11; B. O. Seraphin, in *Semiconductors and Semimetals*, edited by R. K. Willardson and A. C. Beer (Academic, New York, 1970) Vol. VI; D. E. Aspnes and N. Bottka, *ibid.*, Vol. VI; D. F. Blossey and P. Handler, *ibid.*, Vol. IX.

[11]D. A. Dows and A. D. Buckingham, J. Mol. Spectry. 12, 189 (1964); A. D. Buckingham and D. A. Ramsay, J. Chem. Phys. 42, 3721 (1965); N. J. Bridge, D. A. Haner, and D. A. Dows, *ibid.* 44, 3128 (1966); 48, 4196 (1968); D. A. Haner and D. A. Dows, *ibid.* 49, 601 (1968); R. M. Conrad and D. A. Dows, J. Mol. Spectry. 32, 276 (1969).

[12]G. H. Wannier, Phys. Rev. 52, 191 (1937).

[13]G. Dresselhaus, Phys. Chem. Solids 1, 14 (1956).

[14]R. J. Elliott, Phys. Rev. 108, 1384 (1957).

[15]R. J. Elliott, in *Polarons and Excitons*, edited by C. G. Kuper and G. D. Whitfield (Oliver and Boyd, London, 1963), pp. 269 ff.

[16]J. Frenkel, Phys. Rev. 37, 17 (1931); 37, 1276 (1931).

[17]R. E. Peierls, Ann. Physik 13, 905 (1932).

[18]A. W. Overhauser, Phys. Rev. 101, 1702 (1956).

[19]A. S. Davydov, *Theory of Molecular Excitons*, translated by M. Kasha and M. Oppenheimer, Jr. (McGraw-Hill, New York, 1962).

[20]R. S. Knox, in *Solid State Physics, Theory of Excitons*, edited by F. Seitz and D. Turnbull (Academic, New York, 1963) Suppl. 5, .

[21]J. O. Dimmock, in *Optical Properties of* III-V *Compounds*, edited by R. K. Willardson and A. C. Beer (Academic, New York, 1966), Vol. 3, pp. 259 ff.

[22]R. A. Smith, *Semiconductors* (Cambridge U. P., Cambridge, England, 1961), pp. 347, 350, 367, and 410.

[23]C. Hilsum, in *Semiconductors and Semimetals, Physics of* III-V *Compounds*, edited by R. K. Willardson and A. C. Beer (Academic, New York, 1966), Vol. 1, p. 9.

[24]Reference 21, p. 314.

[25]O. Madelung, *Physics of* III-V *Compounds* (Wiley, New York, 1964), p. 101.

[26]B. Segall and D. T. F. Marple, in *Physics and Chemistry of* II-VI *Compounds*, edited by M. Aven and J. S. Prener (Wiley, New York, 1967) pp. 335 and 344.

[27]C. Lanczos, Z. Physik 62, 518 (1930); 68, 204 (1931).

[28]H. Rausch von Traubenberg and R. Gebauer, Z. Physik 54, 307 (1929); 56, 254 (1929); 62, 289 (1930); 71, 291 (1931).

[29]J. R. Oppenheimer, Phys. Rev. 31, 66 (1928).

[30]H. A. Bethe and E. E. Salpeter, *Quantum Mechanics of One and Two Electron Atoms* (Academic, New York, 1957).

[31]W. Franz, Z. Naturforsch. 13, 484 (1958).

[32]L. V. Keldysh, Zh. Eksperim. i Teor. Fiz. 34, 1138 (1958) [Soviet Phys. JETP 7, 788 (1958)].

[33]R. Williams, Phys. Rev. 117, 1487 (1960).

[34]T. S. Moss, J. Appl. Phys. Suppl. 32, 2136 (1962).

[35]K. Tharmalingham, Phys. Rev. 130, 2204 (1963).

[36]J. Callaway, Phys. Rev. 130, 549 (1963); 134, A898 (1964).

[37]W. V. Houston, Phys. Rev. 57, 184 (1940); E. N. Adams, J. Chem. Phys. 21, 2013 (1953); E. O. Kane, J. Phys. Chem. Solids 12, 181 (1959); P. W. Argyres, Phys. Rev. 126, 1386 (1962).

[38]D. E. Aspnes, P. Handler, and D. F. Blossey, Phys. Rev. 166, 921 (1968).

[39]A. Frova and P. Handler, in *Proceedings of the*

*International Conference on the Physics of Semiconductors, Paris*, 1964, edited by M. Huleir (Dunod, Paris, 1964), p. 157.

[40]B. O. Seraphin, in *Proceedings of the International Conference on the Physics of Semiconductors, Paris*, 1964, edited by M. Hulin (Dunod, Paris, 1964), p. 165.

[41]D. E. Aspnes, Phys. Rev. 147, 554 (1966); 153, 972 (1967).

[42]Y. Hamakawa, F. A. Germano, and P. Handler, J. Phys. Soc. Japan Suppl. 21, 111 (1966).

[43]Y. Hamakawa, F. A. Germano, and P. Handler, Phys. Rev. 167, 703 (1968).

[44]B. B. Snavely, Solid State Commun. 4, 561 (1966); Phys. Rev. 167, 730 (1968).

[45]C. Gahwiller and G. Harbeke, Phys. Rev. 185, 1141 (1969).

[46]P. I. Perov, L. A. Avdeeva, and M. I. Elinson, Fiz. Tverd. Tela 11, 541 (1969) [Soviet Phys. Solid State 11, 438 (1969)].

[47]Y. Toyazawa, Progr. Theoret. Phys. (Kyoto) 20, 53 (1958). A Lorentzian shape is predicted for weak exciton-lattice coupling and a Gaussian shape for strong coupling.

[48]P. Handler, S. Jasperson, and S. Koeppen, Phys. Rev. Letters 23, 1387 (1969).

[49]H. A. Antosiewicz, in *Handbook of Mathematical Functions*, edited by M. Abramowitz and I. A. Stegun (U. S. Department of Commerce, Natl. Bur. Std., Washington, D. C., 1964), Appl. Math Ser. 55, 446 ff.

[50]D. F. Blossey (unpublished).

PHYSICAL REVIEW B VOLUME 3, NUMBER 4 15 FEBRUARY 1971

# Nonpairwise Interactions and Vacancy Formation Energies in Simple Molecular Solids†

S. D. Druger

*Department of Physics, College of William and Mary, Williamsburg, Virginia* 23185

(Received 10 June 1970)

A method is given for summing all orders of nonpairwise contributions to the van der Waals interaction energy of a substitutional impurity in a monatomic molecular crystal using a Lorentz oscillator model as an approximation. The nonpairwise contribution to the energy of removing an atom from the lattice is obtained as a limiting case. Applied to rare-gas solids, the model suggests vacancy formation energies reduced from the two-body values, but insufficiently to give complete agreement with experiment.

## I. INTRODUCTION

Calculations using two-body model potentials for the interactions between rare-gas atoms yield third virial coefficients in disagreement with experiment, [1] and predict vacancy formation energies in solid argon and krypton about equal to the cohesive energy per atom, [2–4] while observed thermal vacancy concentrations[5,6] suggest much smaller values. Also, the two-body potentials generally employed predict stability for the hexagonal close-packed (hcp) solid relative to the face-centered cubic (fcc), [7,8] contrary to observation. The possibility of explaining these apparent discrepancies between theory and experiment in terms of nonpairwise contributions to the cohesive energies of rare-gas solids has been widely examined.

Jansen *et al.* [9] consider nonpairwise interactions involving three-atom electron exchange in the overlap region; they obtain rather large three-body contributions (25% of the cohesive energy) that decisively stabilize the fcc lattice, reduce the two-body vacancy formation energy by as much as 47%, [10] and reportedly produce large relaxations around vacancies. [11] Swenberg[12,13] points out, however, that Jansen's effective one-electron Gaussian wave functions give unrealistically large nearest-neighbor overlaps, and that Gaussians with more realistic width parameters produce negligible three-body effects in Jansen's theory. Other possible difficulties with Jansen's approach have also been discussed. [14]

Nonpairwise contributions to the van der Waals interaction energy alone have also been considered. When interatomic overlaps are neglected and a multipole expansion used, the van der Waals interactions among rare-gas atoms are found to be pairwise additive to second order in perturbation theory, [14] and a three-body "triple-dipole" interaction arises in third order. [15–18] The triple-dipole interaction favors the fcc structure, but insufficiently to decisively stabilize it, [18] and Burton[19] shows that it decreases the vacancy formation energy in solid argon, although insufficiently to give agreement with experiment. The triple-dipole interaction also reduces the discrepancies between observed and calculated third virial coefficients in gaseous argon and krypton, [1,20,21] and its possible effects on other rare-gas properties have also been considered. [22–25] Present's calculation[26] suggests that this interaction might be much more significant than three-body interactions arising from overlap and exchange at normal lattice separation.